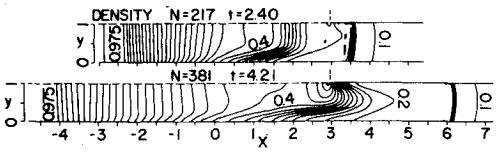

Fig. 5 Isopycnic contours obtained by scheme 2.

with the boundary conditions; for instance, on the wall when using scheme 1

$$\rho_0^{N+1} = \rho_0^N - \{4(\rho v)_1^{N+1} - (\rho v)_2^{N+1}\}\,\Delta t/(2\Delta y),$$

$$T_0^{N+1} = (4T_1^{N+1} - T_2^{N+1})/3$$

where the lower suffices 0, 1, and 2 correspond to $y = 0$, Δy, and $2\Delta y$, respectively.

A time increment when using scheme 1 is determined by the relation

$$\Delta t = 0.25\, Re\, \sigma(\Delta x)^2 \min \rho/\gamma \doteqdot 0.0074$$

which is the upper limit of the von Neumann condition for the parabolic part. The time increment when using scheme 2 is evaluated by the relation

$$\Delta t = 0.7\,\Delta x/\max(|u|+c, |v|+c)$$

which is 0.7 times that of the upper limit of the CFL condition for the hyperbolic part. (The average value of Δt obtained by this evaluation in the numerical experiment was 0.011, which was larger than the value of 0.0074 used for scheme 1. In the provisional calculation by scheme 1 with the same estimate of Δt as used for scheme 2, an instability appeared. Thus, scheme 2 is considered to be more stable than scheme 1.)

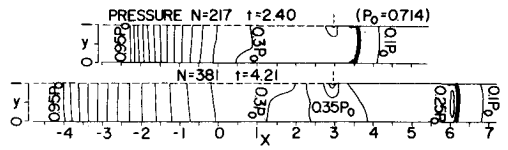

Fig. 6 Isobaric contours obtained by scheme 2.

Results

Isopycnic contours, isobaric contours, iso-velocity contours, and streamlines obtained by scheme 1 are shown in Figs. 1–4, respectively. These figures enable one to follow the unsteady flowfield patterns containing a shock wave, a contact surface, boundary layers and expansion waves numerically. For instance, at $t = 1.61$ the shock wave does not reach the leading edge of the plate, at $t = 2.00$ the shock wave just passes through the edge, at $t = 2.40$ the intermediate point between the shock wave and the contact surface passes the edge at $t = 3.01$ the contact surface reaches the edge, and at $t = 3.40$ and 4.20 complicated flowfield patterns are formed in the vicinity of the edge. These flowfield patterns are qualitatively similar to well-known experimental results. In Figs. 5–8 the isopycnic contours, isobaric contours, iso-velocity contours, and streamlines obtained by scheme 2 are shown. Comparing these with the results obtained by scheme 1, it is found that the flowfield patterns are very similar except for the fact that the shock speed is retarded a little. Since the truncation errors of scheme 1 and scheme 2 at each

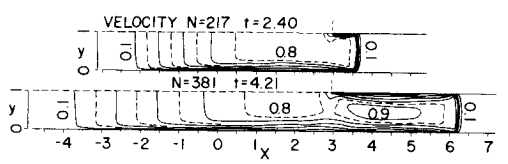

Fig. 7 Iso-velocity contours obtained by scheme 2.

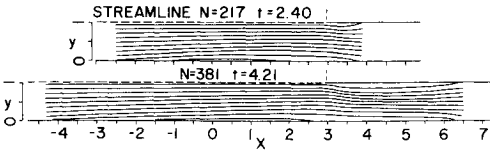

Fig. 8 Streamlines obtained by scheme 2.

step are $0(\Delta t)+0[(\Delta x)^2]$ and $0(\Delta t)+0(\Delta x)+0(\Delta t/\Delta x)$, respectively, when $\Delta x = \Delta y$, the accuracy of scheme 1 is better than that of scheme 2. Consequently, it is thought that the results obtained by scheme 1 are better than those by scheme 2.

It should be noted that the computations by scheme 1 required 230×10^{-5} sec of HITAC 5020F computer time for one time cycle and one node point, while those by scheme 2 required 98.7×10^{-5} sec. The time cycle number required up to $t = 4.2$ was 565 for the scheme 1, while only 381 for scheme 2. Consequently, the computing time of scheme 2 is shorter by a factor of 3.5 than that of scheme 1.

References

[1] Felderman, E. J., "Heat Transfer and Shear Stress in the Shock-Induced Unsteady Boundary Layer on a Flat Plate," *AIAA Journal*, Vol. 6, No. 3, March 1968, pp. 408–412.

[2] Mirels, H., "Correlation Formulas for Laminar Shock Tube Boundary Layer," *The Physics of Fluids*, Vol. 9, 1966, pp. 1265–1272.

[3] Thommen, H. U., "Numerical Integration of the Navier-Stokes Equations," *Zeitschrift für Angewandte Mathematik und Physik*, Vol. 17, 1966, pp. 369–384.

[4] Richtmyer, R. D. and Morton, K. W., *Difference Methods for Initial Value Problems*, 2nd ed., Interscience, New York, 1967, pp. 186–193.

[5] Allen, J. S. and Cheng, S. I., "Numerical Solutions of the Compressible Navier-Stokes Equations for the Laminar Near Wake," *The Physics of Fluids*, Vol. 13, 1970, pp. 37–52.

An Integral Theory for Inviscid, Rotational Flow in Variable Area Ducts

M. SAJBEN*
McDonnell Douglas Corporation, St. Louis, Mo.

A SIMPLE integral theory is presented describing the development of a class of nonuniform initial velocity profiles along a duct of variable cross-sectional area. The calculation applies to steady, incompressible, rotational flows in axisymmetric and two-dimensional passages, assuming zero viscosity. The results may serve as a crude estimate of the effects of gross initial nonuniformities for the case of relatively short ducts with insufficient length for significant boundary layer growth. The crudeness of the model is compensated for by the fact that its use requires trivial computations only, comparable to elementary manipulations of the continuity and Bernoulli equations.

Integration of the continuity equation over the duct cross section yields

$$(d/dx)(R^k \bar{u}) = 0 \qquad (1)$$

Received April 18, 1973; revision received October 19, 1973. This research was conducted under the McDonnell Douglas Independent Research and Development Program.

Index category: Nozzle and Channel Flow.

* Senior Scientist, McDonnell Douglas Research Laboratories. Member AIAA.

In the axisymmetric problem $k = 2$ and R is the radius of the duct, while $k = 1$ and R represents the half width in two-dimensional cases. x is the streamwise coordinate.

After neglecting lateral pressure gradients, integration of the x momentum equation yields

$$(d/dx)(R^k\overline{u^2}) = (R^k/\rho)(dp/dx) \tag{2}$$

Multiplying the x momentum equation by u and integrating, a mechanical energy equation is obtained as

$$(d/dx)\{R^k[\bar{u}(p/\rho)+\tfrac{1}{2}\overline{u^3}]\} = 0 \tag{3}$$

In all cases, the definition of $\overline{u^j}$ is

$$R^k\overline{u^j} = \int_{(k-2)R}^{R} Ku^j r^{k-1}\,dr \tag{4}$$

Next, a two-parameter power law velocity profile is assumed in the form

$$\frac{u}{u_*} = 1 - K\phi\left|\frac{r}{R}\right|^n \tag{5}$$

where r is the lateral coordinate, u_* is the centerline velocity and ϕ is the normalized velocity defect at $r = +R$; both u_* and ϕ are x-dependent parameters. The exponent n is an arbitrary positive constant; in axisymmetric flows the smoothness of the profile requires $n > 1$.

K is a coefficient introduced to unify the analytical treatment of symmetric and antisymmetric velocity profiles. It is defined by

$$K = H(r/R)+(2\sigma-1)H(-r/R) \tag{6}$$

$H(\zeta)$ is the Heaviside function; $H = 1$ for $\zeta > 0$ and $H = 0$ for $\zeta \leqq 0$. σ is an index number; $\sigma = 1$ will result in an even and $\sigma = 0$ in an odd function for $u(r)$.

It is noted that the two-dimensional ducts considered are symmetric with respect to the centerline even though the velocity profiles are allowed to be antisymmetric. In axisymmetric cases an odd profile has no physical meaning, so that $\sigma = 1$ should be taken (which then implies $K = 1$ for all r/R).

Substitution of Eq. (5) into Eq. (4) yields the required three moments of the assumed velocity distribution in the form $\overline{u^j}/u_* = f_j(\phi, n), j = 1, 2, 3$. The f_j are given by the expressions

$$f_1 = 1-\sigma\frac{k}{n+k}\phi \tag{7a}$$

$$f_2 = 1-\sigma\frac{2k}{n+k}\phi+\frac{k}{2n+k}\phi^2 \tag{7b}$$

$$f_3 = 1-\sigma\frac{3k}{n+k}\phi+\frac{3k}{2n+k}\phi^2-\sigma\frac{k}{3n+k}\phi^3 \tag{7c}$$

Note that for two-dimensional, odd profiles $\sigma = 0$ and the expressions are simplified considerably. Using these polynomials in Eqs. (1–3) yields three equations for p, u_* and ϕ which reduce to a single, explicitly integrable, ordinary differential equation for $\phi(A)$ with the following, surprisingly simple solution

$$A^2 = C\phi\left(\phi-\frac{3n+k}{n+k}\right)^{2\sigma}\left(\phi-\frac{n+k}{k}\right)^{-3\sigma} \tag{8}$$

For two-dimensional, odd profiles, $\sigma = 0$ and Eq. (8) simplifies to $A^2 = C\phi$, independent of n. C is an arbitrary constant, determined through specification of $\phi = \phi'$ at the inlet cross section $A = A'$. Equation (8) then defines the velocity defect, ϕ, for any given downstream cross section: $\phi = \phi''$ for $A = A''$. The axial coordinate does not enter because friction and lateral pressure gradients are neglected. Knowing ϕ'', the normalized velocity moments f_j'' can be computed from Eq. (7). The exit centerline velocity is given as

$$u_*'' = \frac{u_*'}{\alpha}\left(\frac{f_1'}{f_1''}\right) \tag{9}$$

and the dimensionless pressure difference between the two ends of the duct is obtained as

$$C_p = \frac{p''-p'}{1/2\rho(\bar{u}')^2} = \frac{f_3'}{(f_1')^3}-\frac{f_3''}{\alpha^2(f_1'')^3}, \tag{10}$$

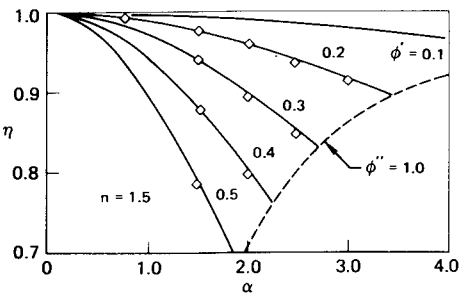

Fig. 1 Effectiveness vs area ratio for axisymmetric ducts. Smooth lines indicate present theory, diamonds are from numerical, inviscid, rotational flowfield computations.

where $f_j = f_j(\phi')$, $f_j'' = f_j(\phi'')$ and $\alpha = A''/A'$. Typical results are presented in Fig. 1 in terms of an effectiveness, η, defined as

$$\eta = C_p/(1-1/\alpha^2) \tag{11}$$

The continuous lines of Fig. 1 show this effectiveness as a function of the exit-inlet area ratio, α, for the selected case of $n = 3/2$. The quantity f_1'' (= ratio of average to peak velocity at the exit) is given in Fig. 2 as a measure of exit nonuniformity.

$\alpha < 1$ corresponds to contraction sections. The f_1'' values show that an increasing contraction ratio gives a flatter profile, a fact well-known since Prandtl. The present calculations give numerical estimates for the degree of flattening for various inlet conditions. If the contractions are acting as nozzles, the conventional nozzle discharge coefficient, K, is related to η through $K = \eta^{-1/2}$. Since $\eta \leqq 1$, the surprising conclusion is that nozzles with nonuniform inlet conditions can have flow coefficients in excess of unity, if viscous effects are negligible.

$\alpha > 1$ represents diffusers. Examination of Eq. (8) shows that any finite value of ϕ' will result in $\phi'' = 1$ (i.e., separation) at some sufficiently large area ratio. All curves are discontinued at this point since the model is not expected to hold for separated flow. The rapidly deteriorating static pressure recovery and the growing exit distortion with increasing area ratio are evident.

The two most important assumptions built into this calculation are the neglect of viscosity and the assumption that the velocity profiles at each station follow Eq. (5).

No theory was found to combine rotational core flow and viscous boundary-layer calculations, which leaves experimental data as the only means of appraising the effects of the inviscid assumption.

Insufficient experimental data precluded a detailed comparison with the present theory. Most experimentors investigate inlet profiles which consist of a potential core and a boundary layer whose thickness is varied by some method. A crude comparison can be made, however, if one postulates that the inlet conditions are adequately characterized by the so-called blockage, B, defined by

$$B = 1-f_1 = 1-(\bar{u}/u_*) \tag{12}$$

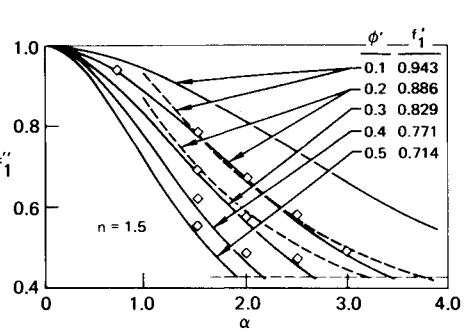

Fig. 2 Ratio of average to peak velocities at duct exit vs area ratio. Smooth lines indicate present theory, diamonds are numerical flowfield computations and dashed lines are calculated from the correlation of Sovran and Klomp.

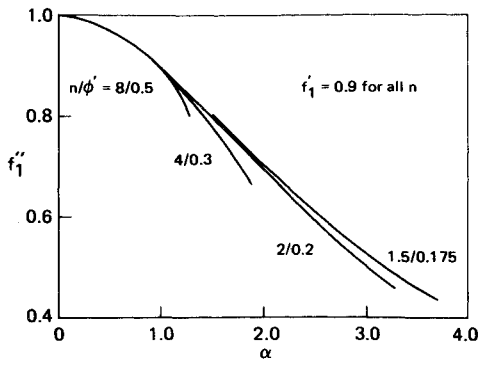

Fig. 3 Ratio of average to peak velocities at duct exit vs area ratio. Combinations of n and ϕ' are such as to keep $f_1' = 0.9 = \text{const}$.

Sovran[1] showed that f_1'' ($= E_2$ in his notation) correlates closely with a quantity defined as $\alpha(100B_1)^{1/4}$ and presents a single empirical curve which correlates well with a large amount of data on conical diffusers. The correlation is expected to hold for diffusers whose area ratio is such that C_p is maximum for a given length/diameter ratio ("optimum" diffusers). Such diffusers are relatively loss-free and are hence most likely to agree with an inviscid theory.

The two dashed lines of Fig. 2 have been calculated from Sovran's correlation (Fig. 22 of Ref. 1). They are to be compared with the top two curves of the family drawn in continuous lines, representing the present results.

The general trends in terms of both α and f_1' are in agreement with the empirical correlation, the measured exit blockage values being greater than the predicted ones. The worst deviation in f_1'' is 0.16, which is roughly twice as much as the data scatter around the correlation curve. Since Sovran's correlation is not claimed to hold for $f_1' \leqq 0.9$, no comparison curves were drawn for lower values.

The comparison of theoretical and empirical results is shown in Fig. 2 only for the arbitrarily chosen exponent of $n = 1.5$. If our postulate that f_1' is adequate to characterize the inlet profile is correct then the choice of n should be irrelevant. This means that the $f_1''(\alpha)$ function should be independent of n. Figure 3 shows that the effect of n (as predicted by this theory) is indeed very weak. Figure 3 refers to $f_1' = 0.9$ only, but other values yield similar plots.

The curves of Fig. 3 are discontinued when ϕ'' reaches unity. The area ratio at which such a "separation" occurs depends strongly on n. This trend is probably not realistic because the location of separation is strongly influenced by the neglected viscous effects.

Our second major assumption concerning the power law shape of the velocity profiles at all stations is tested by comparing present predictions against numerical solutions of the equation

$$\nabla^2\psi = -\omega(\psi) \tag{13}$$

where ψ is the stream function and ω is the vorticity whose dependence on ψ is given through the specification of the inlet velocity profile. The lateral velocity components were assumed zero at the inlet station and the static pressure was assumed constant over the exit plane. The computer program, based on a line relaxation scheme, is from Hoffman.[2] Conical diffuser shapes were used, preceded and followed by three diameter long constant area pipes.

Each diamond in Figs. 1 and 2 represents one such complete flowfield computation. Each is to be compared with the continuous line lying nearest to it. The agreement is clearly very good, indicating that the restriction placed on profile shapes is much less important than the neglect of viscosity.

It is concluded that the presented formulae may be useful for estimation purposes and for describing some velocity profile effects in short, unstalled ducts where pressure forces are dominant.

References

[1] Sovran, G. and Klomp, E. D., "Experimentally Determined Optimum Geometries for Rectilinear Diffusers with Rectangular, Conical or Annular Cross Section," *Fluid Mechanics of Internal Flow*, Elsevier, New York, 1967, pp. 270–319.

[2] Hoffman, G. H., "Rotational Inviscid Flow in Axisymmetric Ducts," Rept. MDC Q0472, 1973, McDonnell Douglas Research Labs., St. Louis, Mo.

A Note on the Shock Standoff Distance for a Spherical Body in Supersonic Flow

T. B. GUY*

Australian Atomic Energy Commission, Lucas Heights, N.S.W., Australia

THE object of this Note is to introduce a simple approximate method of estimating the distance a shock wave stands ahead of a spherical body in supersonic flow. The method assumes that the shock wave is sufficiently close to the body and that it can be considered to be spherical in the neighborhood of the normal in the direction of flow. It is further assumed that the pressure and Mach number conditions shown in the coordinate system in Fig. 1 are precisely those which would apply if the shock wave were produced as a result of an outward-going shock wave undergoing spherical diffraction.

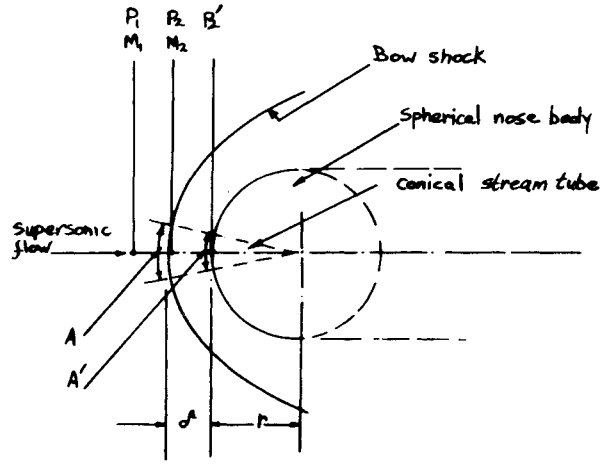

Fig. 1 Sketch of bow shock and spherical body with notation.

With these assumptions, we use the shock strength to ray tube area relationships given by Chisnall[1] as

$$(A/A')^{K(Z_2)} = (Z_2' - 1)/(Z_2 - 1) \tag{1}$$

where $K_{(Z)}$, plotted in Fig. 2, is given by Whitham[2] as

$$K_{(Z)} = 2\left[\left\{\frac{1+2(1-\mu)^2}{(\gamma+1)}\right\}\left\{2\mu+1+\frac{2\gamma}{(\gamma-1)+(\gamma+1)Z}\right\}\right]^{-1} \tag{2}$$

with

$$\mu^2 = [(\gamma+1)+(\gamma-1)Z]/2\gamma Z$$

Received May 24, 1973, revision received October 2, 1973.

Index categories: Supersonic and Hypersonic Flow; Shock Waves and Detonations.

* Engineering Research Division.